MONTANA STATE UNIVERSITY LIBRARY

Curating viscoelastic properties of icosahedral viruses, virus-based nanomaterials, and protein cages

Authors: Ravi Kant, Vamseedhar Rayaprolu, Katilyn McDonald, and Brian Bothner

The final publication is available at Springer via http://dx.doi.org/10.1007/s10867-018-9491-x.

Kant, Ravi, Vamseedhar Rayaprolu, Kaitlyn McDonald, and Brian Bothner. "Curating viscoelastic properties of icosahedral viruses, virus-based nanomaterials, and protein cages." Journal of Biological Physics 44, no. 2 (June 2018): 211-224. DOI:10.1007/s10867-018-9491-x.

Made available through Montana State University's ScholarWorks
scholarworks.montana.edu

Curating viscoelastic properties of icosahedral viruses, virus-based nanomaterials, and protein cages

Ravi Kant[1] · **Vamseedhar Rayaprolu**[2] · **Kaitlyn McDonald**[1] · **Brian Bothner**[1]

Received: 3 January 2018 / Accepted: 16 March 2018 / Published online: 10 April 2018
© Springer Science+Business Media B.V., part of Springer Nature 2018

Abstract The beauty, symmetry, and functionality of icosahedral virus capsids has attracted the attention of biologists, physicists, and mathematicians ever since they were first observed. Viruses and protein cages assemble into functional architectures in a range of sizes, shapes, and symmetries. To fulfill their biological roles, these structures must self-assemble, resist stress, and are often dynamic. The increasing use of icosahedral capsids and cages in materials science has driven the need to quantify them in terms of structural properties such as rigidity, stiffness, and viscoelasticity. In this study, we employed Quartz Crystal Microbalance with Dissipation technology (QCM-D) to characterize and compare the mechanical rigidity of different protein cages and viruses. We attempted to unveil the relationships between rigidity, radius, shell thickness, and triangulation number. We show that the rigidity and triangulation numbers are inversely related to each other and the comparison of rigidity and radius also follows the same trend. Our results suggest that subunit orientation, protein–protein interactions, and protein–nucleic acid interactions are important for the resistance to deformation of these complexes, however, the relationships are complex and need to be explored further. The QCM-D based viscoelastic measurements presented here help us elucidate these relationships and show the future prospect of this technique in the field of physical virology and nano-biotechnology.

Keywords Virus · Icosahedral · QCMD · Viscoelastic · Protein cage

1 Introduction

Icosahedral virus capsids are symmetric supramolecular complexes composed of 100s to 1000s of proteins [1]. They form flexible active containers that can undergo conformational

transitions based on solution and environmental conditions [2, 3]. The geometric arrangement of their subunits imparts a multitude of physical properties that facilitate capsid assembly, maturation, receptor binding, cell entry, and genome release. The icosahedral architecture is stabilized by protein–protein and protein–nucleic acid interactions. Viruses have evolved to accommodate genetic material of varying length by manipulating the arrangement of these proteins and varying the number of subunits that compose a capsid [1, 4]. Interestingly, this symmetric arrangement of proteins is not limited to viruses and can be seen in other cages like ferritins and heat shock proteins [5, 6] with the only difference being the lack of protein–nucleic acid interactions.

Icosahedral viruses are quasi-equivalent, meaning interactions between protein subunits lead to the formation of interchangeable hexameric or pentameric sub-structures in the capsid. Although assembly of viruses does not always follow this hierarchy, the final capsid structure essentially exists in such a quasi-equivalent state. Every icosahedral virus has only 12 such pentameric sub-structures, each present in a specific location determined by the triangulation number (T-number). The T-number is dictated by the equation $h^2 + hk + k^2$ where h and k are the number of steps taken from an assigned pentameric origin (0,0) to the next closest pentameric unit (h,k). h and k cross each other at a 60° angle and are necessarily 0 or positive (Fig. 1a). In the simplest of such cases, a $T = 1$ virus capsid with 60 subunits, each pentamer is directly connected to another pentamer with no hexameric sub-structures present in between. This makes either h or k = 0. In a $T = 3$ capsid (180 subunits or 60 T), h and k are both 1 due to the presence of one hexamer between the pentamers and so on (Fig. 1b). Assuming the size of the subunit remains the same, increasing the number of subunits will increase the T-number and the subsequent volume of the capsid (Fig. 1c). In general, subunit sizes are not similar across viruses and this introduces another layer of complexity in the capsid architecture. This change in subunit size influences not only the T-number but also the diameter, the shell thickness, and the number and nature of subunit-subunit interactions. It is easy to see how these changes might influence the mechanical and, more importantly, biological properties of viruses.

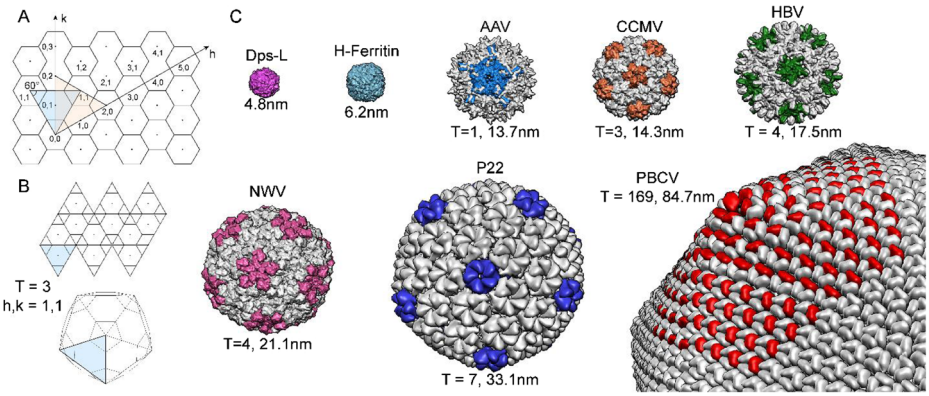

Fig. 1 T-number determination and virus and protein cage library. **a** Flat hexameric sheet showing the positions of h and k and their progression. h and k meet at an angle of 60° and are positive integers. **b** Replacing one of the hexameric units with a pentameric unit results in the introduction of curvature and formation of a convex pentamer (colored subunits in viruses). An example of such replacement (quasi-equivalence) is shown for a $T = 3$ capsid. **c** Fully assembled protein cages and viruses of radii ranging from ~5 to ~90 nm used in this study (shown to scale)

Quartz Crystal Microbalance with Dissipation technology or QCM-D has emerged as a complementary technique to investigate the biomechanical changes in multi-subunit protein complexes [7]. QCM-D is a surface technique that takes advantage of the piezoelectric property of quartz. The gold-coated quartz crystal used in the measurements is driven by applying pulses of alternating current inducing it to oscillate at a resonant frequency (5 MHz for AT-cut crystals). A change in frequency, proportional to the mass change, is observed when a sample is deposited onto the surface of the crystal sensor. When the AC voltage is interrupted, the crystal oscillation decays exponentially, also known as "ringing down". The voltage of oscillatory decay, measured as amplitude over time is approximately at the resonant frequency of the crystal (f_0). This is mixed with a reference frequency (f_R) and filtered with a low pass band filter. The resulting frequency is fit to an exponentially damped sinusoidal wave to obtain the value for dissipation. While the frequency is relative to the mass deposited on the crystal, dissipation is dependent on the viscoelastic properties of the sample. Dissipation is defined as the sum of all energy losses in the system per oscillation (Eq. 1) [8, 9],

$$D = \frac{E_{dissipated}}{2\pi E_{stored}} = \frac{1}{\pi f \tau} \tag{1}$$

where D is dissipation, $E_{\text{dissipated}}$ is the energy lost from the crystal, E_{stored} is the energy retained in the crystal, f is frequency, and the decay constant τ is characteristic of a system and measured in seconds. A small value of τ indicates greater damping, which means the oscillation will decay quickly, while a higher τ represents less damping, hence longer oscillation. Therefore, $\Delta\tau$ represents the change in decay rate and is dependent on the rigidity of the material. Samples that strongly couple to the crystal oscillation contribute less to the dissipation and are classified as relatively rigid materials [9]. Similarly, soft materials show higher deformation and dissipate more energy. By measuring change in frequency and dissipation, QCM-D can detect small-scale and large-scale changes that are associated with the biological functions [7, 10, 11].

Structure and function analyses of icosahedral particles have helped develop a detailed model of these complex assemblages [1, 4]. However, direct measurements of the mechanical properties of particles has only recently been possible [7, 12–14]. Nano-indentation experiments using atomic force microscopy (AFM) on viruses provide the relationship between the force exerted on the capsid and the resultant deformation. This is represented using the force-displacement curves (FDCs), which allow the rigidity of the virus particle to be estimated. FDCs estimate the mechanical strength of the capsids which facilitates a direct comparison between viruses. Although AFM has been the workhorse for such type of measurements, newer technologies attempt to offer a more straightforward and physiologically relevant approach to understanding mechanical properties of viruses. In this study, we employ a powerful complimentary technique, QCM-D, to study the mechanical rigidities of protein cages and viral capsids. QCM-D is a well-established technique that has applications in DNA based sensors, DNA hybridization, DNA–protein interactions, lipid–surface interactions and bioactive surfaces consisting of protein layers (biofilms) [9, 15–21].

QCM-D and AFM are surface-based techniques, however they differ in that QCM-D collects data on a population, whereas AFM is a single-particle-based approach. Both can provide information on the viscoelastic properties of a sample. AFM as a scanning probe microscope directly measures the force between a probe and the object. The response of the object to the applied force is a direct readout of the viscoelastic properties and can be used to

calculate Young's modulus [22–24]. QCM-D also provides information on viscoelastic properties, however, converting this into quantitative values involves complex modeling that takes into account the interaction of acoustic waves with the sample and the solvent [9]. AFM can also provide information on deformation, failure, and of course high-resolution images. The interaction between sample and surface must be taken into consideration for both techniques. For AFM, this has been investigated and can lead to deformation of particles [25–27]. We expect similar deformations may occur in QCM-D.

QCM-D has been used previously to study multilayer assemblages of LiDPS [28] and CPMV [29]. Our group was the first to use QCM-D to detect and elucidate structural changes during expansion and functionalization of Cowpea chlorotic mottle virus (CCMV) [7]. Here, we expand our previous work to include a variety of cages from non-icosahedral to icosahedral symmetry to understand their architectural differences. The viral and protein platforms studied here have been isolated from a range of different species, including algae, bacteria, moths, plants, and primates, and portray the diversity of these supramolecular complexes. Along with diversity in their host range, these complex platforms also represent a complicated interplay of their T-numbers, cage size, protein–protein and protein–nucleic acid interactions and overall amino acid composition. To understand and compare the viscoelastic properties of such mosaic platforms, we provide the first instance of a carefully curated library of different viruses and protein cages (Fig. 1c) using QCM-D. To also expand our understanding about nano-assemblages, protein cages that were much smaller than the viruses were included in the analysis. Our study points to a complex relationship that governs rigidity. QCM-D experiments excel at mimicking physiological conditions and this feature acts as a key strength along with the speed of experimentation. QCM-D facilitates a quantifiable approach in which rigidity is directly compared to T-numbers, protein shell thickness and radius, and conclusions can be drawn about how they are influenced by their subunit interactions. While our D300 instrument could only analyze a single sample at a time, future iterations have incorporated four sensors in one instrument along with electrochemistry modules thereby vastly expanding the abilities of the technique. QCM-D also provides the advantage of ease of use and a very straightforward analysis compared to most biophysical techniques. Although QCM-D results can be misinterpreted if bulk buffer effects are not considered, this does not present a significant challenge for most biological samples if proper controls are conducted. Our work shows that QCM-D can be used as a common platform to not only compare biological entities among themselves but also with their nanomaterial counterparts while providing insights into both biology and material design.

2 Materials and methods

2.1 QCM-D data collection

The viscoelastic properties of different protein cages were explored by using QCM-D (Q-Sense D300 system, Q-Sense AB, Gothenburg, Sweden). For these measurements, gold-coated quartz crystals (AT cut) with a fundamental resonant frequency of 5 MHz were used. Baseline was established with their respective storage buffers and recorded for 10 min. Each sample (0.01 mg/ml, 0.6 ml) were then gradually deposited on the crystal and allowed to stabilize for 45 min. To remove the loosely bound viral particles, the gold surface was then washed with 0.6 ml of the same buffer for 10 min. For *Nudaurelia capensis* omega virus

(NωV) only, after the wash step, another buffer exchange step with pH 5.0 buffer was introduced and the samples were allowed to incubate for 2 h. Buffer exchange control was run to consider the buffer exchange effect. Error bars for rigidities were generated using standard deviations and represent at least three replicates.

After every run, the gold surface was cleaned and regenerated by soaking the crystal in a 1:1:5 mixture of H_2O_2 (30%), NH_3 (25%), and distilled water at 60 °C for 15 min followed by exposure to UV light in UV chamber for 10 min. All samples were run in random order in triplicate and each time fresh cleaned crystal was used. Frequency and dissipation values were obtained at fundamental frequency 5 MHz and three overtones (15, 25, and 35 MHz). Rigidities were calculated by taking the ratio of change in frequency to change in dissipation $|\Delta F/\Delta D|$.

2.2 Data analysis

All QCM-D data analysis was done as described previously using the Q-soft software from Biolin Scientific [7]. T-numbers and radii were obtained from ViperDB [30]. All plots and exponential fits were made in Igor Pro 6.3 and final figures were made in Adobe Illustrator .

3 Results

3.1 Rigidity and T-number are inversely related

Previous experiments with CCMV showed that QCM-D could be used to elucidate conformational differences in virus particles [7]. Here, we expanded QCM-D to explore changes in the other viruses (infecting different hosts) and protein cages. Samples were allowed to adsorb onto an oscillating gold-coated quartz crystal and changes in frequency and dissipation were measured for each. In QCM-D, the observed frequency is dependent on the mass absorbed to the surface. Dissipation is related to the deformation and viscoelasticity of the attached sample layer. Thus, QCM-D measures two independent properties [9]. Since QCM-D is a population-based measurement, by taking the ratio of change in frequency and dissipation, qualitative comparisons of average rigidity of the adsorbed material can be made. A ratio of the change in frequency to change in dissipation ($|\Delta f/\Delta D|$) for a sample is a measure of its rigidity where higher ratios correspond to higher rigidities. We calculated the ratios for all samples and plotted the trend against their T-numbers (Fig. 2). We noticed a decrease in rigidity with increase in T-number. The exceptions to this were the closed and swollen forms of CCMV (cCCMV and sCCMV, respectively), which negatively deviated from the general trend. We also noticed that viruses that shared the same T-number such as the AAV serotypes showed significant differences while still fitting into the trend. Similarly, HBVtrunc, which is a truncated version of the wild-type hepatitis B virus and shares the same T-number, also showed a marked reduction in rigidity compared to its wild-type counterpart.

3.2 Rigidity is influenced by both shell thickness and particle radius

T-numbers give us a coarse perspective of how virus capsids respond to external shearing forces but fall short when comparing capsids of the same T-number. Also, it is not possible to compare protein cages or extensively modified virus particles due to unavailability or possible

distortion of their T-numbers due to the modifications. With this in mind, we next investigated the effect of shell radius (Fig. 3) and thickness on rigidity. To visualize this, we plotted shell radius vs. rigidity and shell thickness vs. rigidity separately. We noticed a clear exponential decrease in rigidity with increase in shell radius, similar to that observed with T-numbers (Fig. 4). The shell thickness vs. rigidity plot showed more outliers, although it still followed a weak exponentially decreasing trend (Fig. 4b). It was evident from this initial analysis that both the radius and thickness influenced rigidity in similar ways. We also included two functionalized CCMV capsids (XCCMV and MXCCMV) and two protein cages (DpsL and H-ferritin) in this comparison. XCCMV and MXCCMV both are glutaraldehyde crosslinked CCMV samples, the only difference being the replacement of genomic RNA with a polyoxomolybdate mineral core in MXCCMV. DpsL is a ~10 nm, dodecameric cage-like particle isolated from the hyperthermophilic archaeal species *Sulfolobus solfataricus* while human H-ferritin is ~12 nm in size and self-assembles with an octahedral symmetry. The crosslinked CCMV samples showed drastically higher rigidities with MXCCMV being the highest among all the samples tested and ~ 4 times higher than its unmodified native counterpart. DpsL and H-ferritin also showed significantly higher rigidities than any of the viruses tested. It is also interesting to note that PBCV-1, a 170-nm, $T = 169$ chlorella virus, and the chlorella family of viruses show very similar rigidities and the lowest rigidities among all samples.

4 Discussion

While T-number is a straight-forward way to describe capsid architecture, there are subtle and not-so-subtle differences that this does not account for. For example, adeno-associated viruses (AAV) are $T = 1$ capsids that are now approved for gene therapy [31, 32]. Each capsid is made up of three alternatively spliced viral proteins (VP1, VP2, VP3) in a ratio of 1:1:8–10. The sequence similarity among the AAV serotypes tested here ranges from 54 to 84%. Our experiments show that the rigidities of AAV capsids vary significantly with serotype. Thermal and proteolytic stabilities of empty and genome filled AAVs have also been well studied and have shown similar differences [33, 34]. On the other hand, nanoindentation studies of AAV capsids using AFM pointed to a higher propensity for deformation of the empty forms [35]. Delineating these

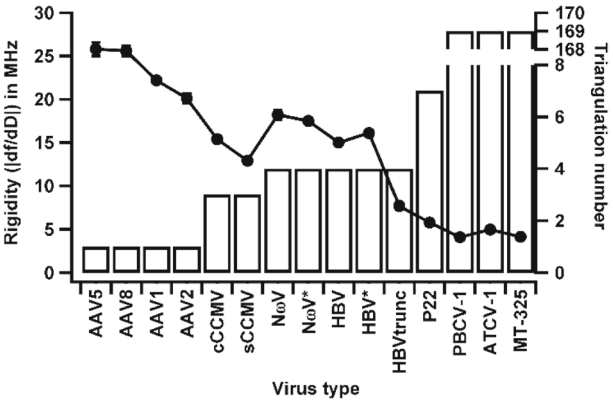

Fig. 2 Rigidity vs. T-number. Rigidity and T-number plotted for each virus tested. Rigidities decrease with increase in T-number with CCMV samples being the exceptions. Protein cages were not included due to the lack of an assigned T-number

seemingly opposing differences in behavior using only T-numbers could lead to misleading interpretations. The use of shell radius and thickness in conjunction with T-number provides us with a robust set of parameters that are affected by the comprehensive structural and dynamic transitions that capsids experience. While AAV and CCMV have similar radii, their T-numbers, shell thicknesses, and rigidities are different. In comparison, the AAV capsid has a higher shell thickness and the subunit protein is 3–4 times higher in molecular weight. It is important to note that CCMV (both closed and swollen forms) have native RNA in them and yet AAVs, both empty and genome-filled, have been shown to have significantly higher thermal stabilities [33, 34, 36] and stiffness [13, 35, 37] compared to CCMV. Our results corroborate with these previous observations.

HBV is a $T = 4$, enveloped double-stranded DNA virus and is the cause for hepatitis B-induced liver cirrhosis and cancer, a major global health problem. The inner nucleocapsid core is assembled from 240 copies of the capsid protein. An in vitro assembled empty core was used in our study and compared to two other mutants, HBV*, which incorporates three serine-to-glutamate mutations, which impair phosphorylation of its C-terminal domain (CTD) [38] and HBVtrunc, which lacks 34 residues in the CTD. The serine-to-glutamate mutations impart a higher proteolytic and thermal stability to HBV* [39]. In our study, we observed slightly higher rigidity (~7%) with the HBV* compared to HBV indicating a slightly more mechanically resistant capsid. Of the 34 residues in the CTD, 16 are arginines and seven are serines. Modification of the serines to glutamates (HBV*) not only disrupts phosphorylation but may also act to neutralize some of the arginines and help stabilize subunit interactions [39]. This is consistent with the small, but significant, increase in particle rigidity. When the CTD is completely removed, as in the case of HBVtrunc, a more drastic reduction in rigidity occurs (~48%) with little perturbation of the structure. These results strongly suggest that the CTD enhances rigidity by improving interactions among coat protein subunits. They also show the importance of post-translational modifications on capsid structure and dynamics. Thus, HBV is a relevant example where the effects of both simple amino-acid modifications and large-scale domain level deletions can be elucidated using QCM-D.

A different type of effect can be seen with NωV, another $T = 4$ virus considered a model for single-stranded RNA viruses. The procapsid form of the virus, 24 nm (NωV*), has a 644-

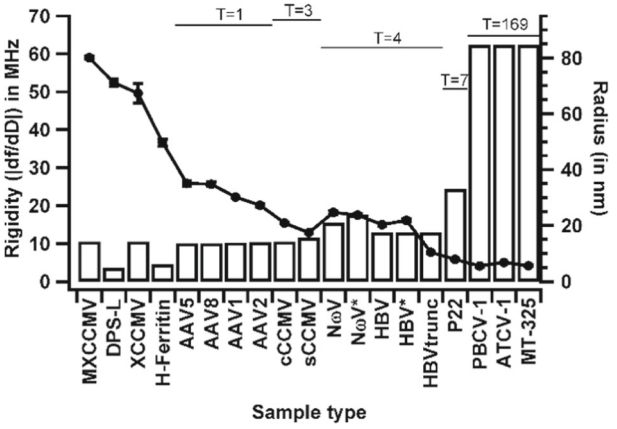

Fig. 3 Rigidity vs. radius. Rigidity and radius of each sample were plotted for each sample type. With an increase in the radius, the rigidity decreased. Two extensively modified CCMV capsids were also included. Rigidity, T-number, and radius values of all samples are included in Table 1

Table 1 QCM-D library of different viruses and protein cages

Sample	Radius	Rigidity (|df/dD|)	T-number	Number of subunits	Natural genome	Genome present in sample	Host/derived from
Dps-L	4.8	52.4 ± 1	–	10	–	–	*Sulfolobus solfataricus*
H-Ferritin	6.2	36.6 ± 0.9	–	12	–	–	Human
AAV5	13.7	25.8 ± 0.8	1	60	ssDNA	No	Human
AAV8	13.7	25.6 ± 0.6	1	60	ssDNA	No	Human
AAV1	13.9	22.2 ± 0.2	1	60	ssDNA	No	Human
AAV2	14	20.1 ± 0.5	1	60	ssDNA	No	Human
cCCMV	14.3	15.4 ± 0.1	3	180	ssRNA	Yes	Legumes
sCCMV	15.7	12.9 ± 0.2	3	180	ssRNA	Yes	Legumes
HBV	17.5	15 ± 0.3	4	240	dsDNA	No	Human
HBV*	17.5	16.1 ± 0.4	4	240	dsDNA	No	Human
HBVtrunc	17.5	7.7 ± 0.2	4	240	dsDNA	No	Human
NωV	21.1	18.2 ± 0.5	4	240	ssRNA	No	Insects
NωV*	24	17.5 ± 0.3	4	240	ssRNA	No	Insects
P22	33.1	5.8 ± 0.1	7	420	dsDNA	Yes	*Salmonella typhimurium*
PBCV-1	84.7	4.1 ± 0.3	169	5040	dsDNA	Yes	Green alga *Chlorella* species
ATCV-1	84.7	4.9 ± 0.03	169	5040	dsDNA	Yes	Green alga *Chlorella* species
MT-325	84.7	4.1 ± 0.16	169	5040	dsDNA	Yes	Green alga *Chlorella* species

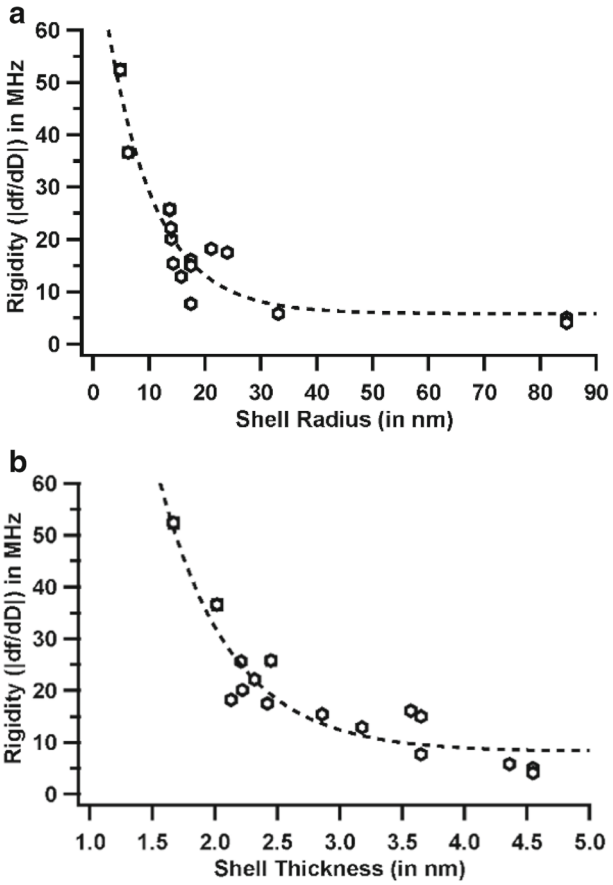

Fig. 4 **a** Rigidity vs. radius. A plot of rigidity vs. radius revealed a strong exponential trend. The points were fit to a single exponential. **b** Rigidity vs. shell thickness. A plot of rigidity vs. shell thickness revealed a weak exponential trend. The dotted line shows a single exponential fit to the data

amino-acid subunit that undergoes proteolytic cleavage at residue 570, resulting in the mature capsid (NωV, 21 nm). This cleavage event occurs post viral assembly, releasing a γ-peptide [40]. The rigidities of NωV and NωV*, both devoid of genome, vary only by ~ 4%, suggesting that even a concerted large-scale deletion and reduction in diameter does not alter the virus behavior by much. The lack of genome also suggests that all the necessary protein–protein interactions for the stabilization of the virus have already been accomplished at the procapsid stage. This stabilization has been previously proposed and is due to the electrostatic repulsions between the numerous deprotonated acidic charges present on the surface of the capsid protein at high pH [40]. The γ-peptide does not play a role in stability, but cleavage is a molecular switch that locks the capsid in the mature conformation and untethers the peptide to interact with cell membranes, as is the case with another insect virus (FHV) [41].

P22 bacteriophage has been developed extensively as a versatile nanomaterial [42–44]. The infectious mature particle used in this study is a $T = 7$ virus with a ~ 33-nm radius. The assembly process of P22 involves dsDNA being energetically driven by a portal structure into a fully formed capsid. This is markedly different from the other viruses studied here whose subunits either self-assemble around the genome [45] or the genome is replicated inside a fully formed capsid [46]. This

headful packaging mechanism, common in dsDNA bacteriophages, creates pressures upwards of 60 atm (6 MPa) inside the capsids, which are important for genome release during infection [47]. Force constant obtained from AFM nanoindentations of extraneously loaded P22 capsids [48] is much lower than that of AAV [35] while the absence of this cargo reduces it further [25]. P22 on the QCM-D shows a very similar behavior with much lower rigidities compared to AAV. This suggests that even while existing as a highly pressurized capsid, P22 can still be isovolumetrically distorted to a greater extent than the rigid AAV capsid by the shear forces of the liquid. Thermal and proteolytic stabilites of AAVs have shown that these capsids are extremely resistant to environmental changes [33, 34] and our QCM-D results substantiate these results. The low rigidity of PBCV among compared to other viruses was expected due to the greater diameter and emphasizes that rigidity is not a simple outcome of subunit number. Rather, it is a complex combination of subunit number, orientation, and interaction strength.

FVK is a universal, non-dimensional parameter used to estimate buckling propensity of spheres with thin shells due to mechanical stresses. Specifically with respect to capsids, a critical threshold for FVK ($\gamma = 154$) was proposed by Lidmar et al. to define when a capsid would transition from a spherical to a more faceted shape, called asphericity [27]. This faceting is caused by disclination at the 12 isolated five-fold symmetry axes. These pentameric units experience high strain and thereby adopt a conical shape. FVK is described by Eq. (2), where Y is Young's modulus, R is the radius of the shell, κ is the bending rigidity, ν is the Poisson's ratio, d is the shell thickness.

$$\gamma = YR^2/\kappa = 12\left(1-\nu^2\right)(R/d)^2 \tag{2}$$

From the equation, it is evident that FVK is dependent on the radius and shell thickness. Previous modeling and experimental studies have tried to explain the mechanical properties of viruses using Föppl Von Kármán number (FVK,γ). These studies assumed that the thickness of the shell does not have an impact on the mechanical properties. Experimental work could not find consistent correlation due to the inherent heterogeneity of these shells and the consequent failure of the thin shell approximation. These studies brought into light the innate complexity of these protein shells and especially the dependence of mechanical properties radius and shell thickness. We see this dependence very clearly with our QCM-D data when we plot a ratio of (radius/thickness)^2 to the rigidity (Fig. 5). It is imperative to note that the

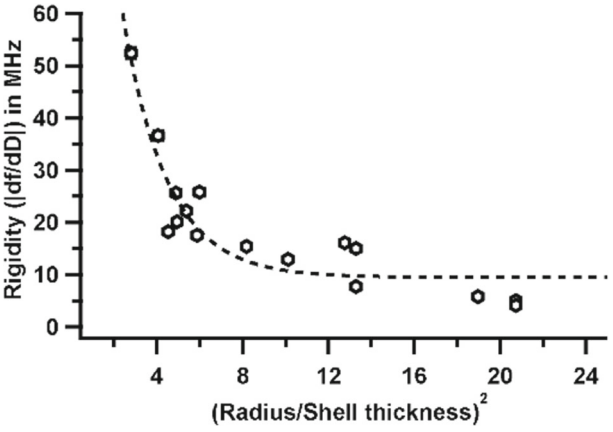

Fig. 5 Rigidity vs. $(R/d)^2$

rigidity values reported here may not correlate well with FVK numbers for smaller viruses like CCMV and AAV. This discrepancy was first observed by Klug et al. [49] in their mechanical models. Nevertheless, the rigidity values of these smaller viruses still fit our overall hypothesis and let us draw logical and accurate conclusions. In addition, although there may be a direct dependence of rigidity on radius and thickness, it is imperative to consider other properties of protein shell structure to attain a practical understanding. In this regard, a recent study involving simulations driven by AFM nanoindentation data from 35 different viruses [50] examined the dependence of mechanical properties on several different factors including shell thickness. Cieplak et al. used AFM nanoindentation modeling, which assumes that the virus is subjected to spatially targeted stress. They found no correlation between mechanical properties and virus size or symmetry. At first, this may seem to disagree with our findings because we note a correlation between rigidity and size/symmetry, but they found a compelling connection between mechanical properties and coordination number (mean number of interactions to neighboring amino acids). Therefore, our study supports their interpretation that protein–protein interaction is a key parameter with respect to mechanical properties. Our population-based QCM-D measurements extend the finding of in silico modeling and suggests that rigidity is a function of T-number, shell radius, shell thickness, and most importantly the protein–protein and protein–nucleic acid interactions in the subunits.

The QCM-D results presented here follow similar trends demonstrated with AFM and AFM simulations [13, 35, 50, 51]. However, there are several areas in which the power of QCM-D shines. QCM-D values are generated in near physiological conditions where the samples are being subjected only to shear forces by the liquid medium, as would be the case in biological systems. We also demonstrate that with minimal changes to the measurement protocols, we are able to measure virus particles with very different properties (Ex: XCCMV and MXCCMV) without compromising speed or reproducibility. This positions QCM-D as a semi-high-throughput method for viral particle and protein cage characterization. While rigidity obtained from simple QCM-D analysis is central to the technique, QCM-D can also be used to determine the thickness of the material layer being analyzed, making this a powerful tool for the analysis of biological composite materials as well [28] and carefully designed thin films with desired properties [29]. These are essential details needed for material synthesis using biological components. The application of QCM-D technology for the biophysical analysis of large protein structures has been largely unexplored. Our curated library attempts to bring into light the straight-forward nature of the QCM-D technique and its ability to quantitatively characterize physical properties of biomaterials. Such complementary information obtained in real-time, in close to physiological conditions, with high precision, and a minimum of effort will be of great benefit for biologists, chemists, and physicists alike.

Acknowledgements We thank Dr. Matthew Dixon from Biolin Scientific for technical assistance. We also thank Ms. Neerja Zambare for insightful discussions. We thank Drs. David D Dunnigan, James L. Van Etten, Trevor Douglas, John E. Johnson, Adam Zlotnick, and Mavis McKenna for providing the samples for this analysis. This project was funded in part by NIH AAV grant R01 AI081961-01A1 to BB.

References

1. Caspar, D.L.D., Klug, A.: Physical principles in the construction of regular viruses. Basic Mech. Anim. Virus Biol. **27**, 1–24 (1962)
2. Fricks, C.E., Hogle, J.M.: Cell-induced conformational change in poliovirus: externalization of the amino terminus of VP1 is responsible for liposome binding. J. Virol. **64**, 1934–1945 (1990)

3. Bothner, B., Schneemann, A., Marshall, D., Reddy, V., Johnson, J.E., Siuzdak, G.: Crystallographically identical virus capsids display different properties in solution. Nat. Struct. Mol. Biol. **6**, 114–116 (1999). https://doi.org/10.1038/5799
4. Johnson, J.E., Speir, J.: Quasi-equivalent viruses: a paradigm for protein assemblies. J. Mol. Biol. **269**, 665–675 (1997). https://doi.org/10.1006/jmbi.1997.1068
5. Gauss, G.H., Benas, P., Wiedenheft, B., Young, M., Douglas, T., Lawrence, C.M.: Structure of the DPS-like protein from *Sulfolobus solfataricus* reveals a bacterioferritin-like dimetal binding site within a DPS-like dodecameric assembly. Biochemistry **45**, 10815–10827 (2006). https://doi.org/10.1021/bi060782u
6. Lawson, D.M., Artymiuk, P.J., Yewdall, S.J., Smith, J.M., Livingstone, J.C., Treffry, A., Luzzago, A., Levi, S., Arosio, P., Cesareni, G.: Solving the structure of human H ferritin by genetically engineering intermolecular crystal contacts. Nature **349**, 541–544 (1991). https://doi.org/10.1038/349541a0
7. Rayaprolu, V., Manning, B.M., Douglas, T., Bothner, B.: Virus particles as active nanomaterials that can rapidly change their viscoelastic properties in response to dilute solutions. Soft Matter **6**, 5286 (2010). https://doi.org/10.1039/c0sm00459f
8. Dutta, A.K., Belfort, G., Dutta, A.K., Belfort, G.: Adsorbed gels versus brushes: viscoelastic differences. Langmuir **23**, 3088–3094 (2007). https://doi.org/10.1021/la0624743
9. Dixon, M.C.: Quartz crystal microbalance with dissipation monitoring: enabling real-time characterization of biological materials and their interactions. J. Biomol. Tech. **19**, 151–158 (2008)
10. Rydell, G.E., Dahlin, A.B., Höök, F., Larson, G.: QCM-D studies of human norovirus VLPs binding to glycosphingolipids in supported lipid bilayers reveal strain-specific characteristics. Glycobiology **19**(11), 1176–1184 (2009)
11. da Silva, A.K., Kavanagh, O.V., Estes, M.K., Elimelech, M.: Adsorption and aggregation properties of norovirus GI and GII virus-like particles demonstrate differing responses to solution chemistry. Environ. Sci. Technol. **45**, 520–526 (2011). https://doi.org/10.1021/es102368d
12. Ivanovska, I.L., de Pablo, P.J., Ibarra, B., Sgalari, G., MacKintosh, F.C., Carrascosa, J.L., Schmidt, C.F., Wuite, G.J.L.: Bacteriophage capsids: tough nanoshells with complex elastic properties. Proc. Natl. Acad. Sci. U. S. A. **101**, 7600–7605 (2004). https://doi.org/10.1073/pnas.0308198101
13. Gibbons, M., Klug, W.: Nonlinear finite-element analysis of nanoindentation of viral capsids. Phys. Rev. E **75**, 031901 (2007). https://doi.org/10.1103/PhysRevE.75.031901
14. Roos, W.H., Wuite, G.J.L.: Nanoindentation studies reveal material properties of viruses. Adv. Mater. **21**, 1187–1192 (2009). https://doi.org/10.1002/adma.200801709
15. Nguyen, T.H., Elimelech, M.: Adsorption of plasmid DNA to a natural organic matter-coated silica surface: kinetics, conformation, and reversibility. Langmuir **23**, 3273–3279 (2007). https://doi.org/10.1021/la0622525
16. Nguyen, T.H., Chen, K.L.: Role of divalent cations in plasmid DNA adsorption to natural organic matter-coated silica surface. Environ. Sci. Technol. **41**, 5370–5375 (2007). https://doi.org/10.1021/es070425m
17. Nguyen, T.H., Elimelech, M.: Plasmid DNA adsorption on silica: kinetics and conformational changes in monovalent and divalent salts. Biomacromolecules **8**, 24–32 (2007). https://doi.org/10.1021/bm0603948
18. Keller, C., Kasemo, B.: Surface specific kinetics of lipid vesicle adsorption measured with a quartz crystal microbalance. Biophys. J. **75**, 1397–1402 (1998). https://doi.org/10.1016/S0006-3495(98)74057-3
19. Cho, N.J., Cho, S.J., Kwang, H.C., Glenn, J.S., Frank, C.W.: Employing an amphipathic viral peptide to create a lipid bilayer on au and TiO2. J. Am. Chem. Soc. **129**, 10050–10051 (2007). https://doi.org/10.1021/ja0701412
20. Schofield, A.L., Rudd, T.R., Martin, D.S., Fernig, D.G., Edwards, C.: Real-time monitoring of the development and stability of biofilms of *Streptococcus mutans* using the quartz crystal microbalance with dissipation monitoring. Biosens. Bioelectron. **23**, 407–413 (2007). https://doi.org/10.1016/j.bios.2007.05.001
21. Wittmer, C.R., Phelps, J.A., Saltzman, W.M., Van Tassel, P.R.: Fibronectin terminated multilayer films: protein adsorption and cell attachment studies. Biomaterials **28**, 851–860 (2007). https://doi.org/10.1016/j.biomaterials.2006.09.037
22. Moreno-Madrid, F., Martín-González, N., Llauró, A., Ortega-Esteban, A., Hernando-Pérez, M., Douglas, T., Schaap, I.A.T., de Pablo, P.J.: Atomic force microscopy of virus shells. Biochem. Soc. Trans. **45**, 499–511 (2017). https://doi.org/10.1042/BST20160316
23. Llauro, A., Schwarz, B., Koliyatt, R., Douglas, T.: Tuning viral capsid nanoparticle stability with symmetrical morphogenesis. (2016). https://doi.org/10.1021/acsnano.6b03441
24. Llauró, A., Guerra, P., Irigoyen, N., Rodríguez, J.F., Verdaguer, N., De Pablo, P.J.: Mechanical stability and reversible fracture of vault particles. Biophys. J. **106**, 687–695 (2014). https://doi.org/10.1016/j.bpj.2013.12.035
25. Llauro, A., Schwarz, B., Koliyatt, R., de Pablo, P.J., Douglas, T.: Tuning viral capsid nanoparticle stability with symmetrical morphogenesis. ACS Nano **10**(9), 8465–8473 (2016). https://doi.org/10.1021/acsnano.6b03441

26. Zeng, C., Hernando-Pérez, M., Dragnea, B., Ma, X., van der Schoot, P., Zandi, R.: Contact mechanics of a small icosahedral virus. Phys. Rev. Lett. **119**, 38102 (2017). https://doi.org/10.1103/PhysRevLett.119.038102
27. Llauró, A., Schwarz, B., Koliyatt, R., de Pablo, P.J., Douglas, T.: Tuning viral capsid nanoparticle stability with symmetrical morphogenesis. ACS Nano **10**, 8465–8473 (2016). https://doi.org/10.1021/acsnano.6b03441
28. Kang, S., Suci, P., Broomell, C.C., Iwahori, K., Kobayashi, M., Yamashita, I., Young, M., Douglas, T.: Janus-like protein cages. Spatially controlled dual-functional surface modifications of protein cages. Nano Lett. **9**, 2360–2366 (2009). https://doi.org/10.1021/nl9009028
29. Steinmetz, N.F., Findlay, K.C., Noel, T.R., Parker, R., Lomonossoff, G.P., Evans, D.J.: Layer-by-layer assembly of viral nanoparticles and polyelectrolytes: the film architecture is different for spheres versus rods. Chembiochem **9**, 1662–1670 (2008). https://doi.org/10.1002/cbic.200800070
30. Carrillo-Tripp, M., Shepherd, C.M., Borelli, I.A., Venkataraman, S., Lander, G., Natarajan, P., Johnson, J.E., Brooks, C.L., Reddy, V.S.: VIPERdb2: an enhanced and web API enabled relational database for structural virology. Nucleic Acids Res. **37**, D436–D442 (2009). https://doi.org/10.1093/nar/gkn840
31. Grimm, D., Kay, M.: From virus evolution to vector revolution: use of naturally occurring serotypes of adeno-associated virus (AAV) as novel vectors for human gene therapy. Curr. Gene Ther. **3**, 281–304 (2003)
32. Van Vliet, K.M., Blouin, V., Brument, N., Agbandje-McKenna, M., Snyder, R.O., Van Vliet, K.M., Blouin, V., Brument, N., Agbandje-McKenna, M., Snyder, R.O., Van Vliet, K.M., Blouin, V., Brument, N., Agbandje-McKenna, M., Snyder, R.O.: The role of the adeno-associated virus capsid in gene transfer. Methods Mol. Biol. **437**, 51–91 (2008). https://doi.org/10.1007/978-1-59745-210-6_2
33. Rayaprolu, V., Kruse, S., Kant, R., Venkatakrishnan, B., Movahed, N., Brooke, D., Lins, B., Bennett, A., Potter, T., McKenna, R., Agbandje-McKenna, M., Bothner, B.: Comparative analysis of adeno-associated virus capsid stability and dynamics. J. Virol. **87**, 13150–13160 (2013). https://doi.org/10.1128/JVI.01415-13
34. Bennett, A., Patel, S., Mietzsch, M., Jose, A., Lins-Austin, B., Yu, J.C., Bothner, B., McKenna, R., Agbandje-McKenna, M.: Thermal stability as a determinant of AAV serotype identity. Mol. Ther. Methods Clin. Dev. **6**, 171–182 (2017). https://doi.org/10.1016/j.omtm.2017.07.003
35. Zeng, C., Moller-Tank, S., Asokan, A., Dragnea, B.: Probing the link among genomic cargo, contact mechanics, and nanoindentation in recombinant adeno-associated virus 2. J. Phys. Chem. B **121**, 1843–1853 (2017). https://doi.org/10.1021/acs.jpcb.6b10131
36. Willits, D., Zhao, X., Olson, N., Baker, T.S., Zlotnick, A., Johnson, J.E., Douglas, T., Young, M.J.: Effects of the cowpea chlorotic mottle bromovirus $\hat{I}^2$-hexamer structure on virion assembly. Virology **306**, 280 (2003)
37. Roos, W.H., Bruinsma, R., Wuite, G.J.L.: Physical virology. Nat. Phys. **6**, 733–743 (2010). https://doi.org/10.1038/nphys1797
38. Wang, J.C.-Y., Dhason, M.S., Zlotnick, A.: Structural organization of pregenomic RNA and the carboxy-terminal domain of the capsid protein of hepatitis B virus. PLoS Pathog. **8**, e1002919 (2012). https://doi.org/10.1371/journal.ppat.1002919
39. Selzer, L., Kant, R., Wang, J.C.-Y.Y., Bothner, B., Zlotnick, A.: Hepatitis B virus core protein phosphorylation sites affect capsid stability and transient exposure of the C-terminal domain. J. Biol. Chem. **290**, 28584–28593 (2015). https://doi.org/10.1074/jbc.M115.678441
40. Matsui, T., Lander, G., Johnson, J.E.: Characterization of large conformational changes and autoproteolysis in the maturation of a T=4 virus capsid. J. Virol. **83**, 1126–1134 (2009). https://doi.org/10.1128/JVI.01859-08
41. Banerjee, M., Khayat, R., Walukiewicz, H.E., Odegard, A.L., Schneemann, A., Johnson, J.E.: Dissecting the functional domains of a nonenveloped virus membrane penetration peptide. J. Virol. **83**, 6929–6933 (2009). https://doi.org/10.1128/JVI.02299-08
42. Jordan, P.C., Patterson, D.P., Saboda, K.N., Edwards, E.J., Miettinen, H.M., Basu, G., Thielges, M.C., Douglas, T.: Self-assembling biomolecular catalysts for hydrogen production. Nat. Chem. **8**, 179–185 (2016). https://doi.org/10.1038/nchem.2416
43. Zhou, Z., Bedwell, G.J., Li, R., Bao, N., Prevelige, P.E., Gupta, A.: P22 virus-like particles constructed Au/CdS plasmonic photocatalytic nanostructures for enhanced photoactivity. Chem. Commun. **51**, 1062–1065 (2015). https://doi.org/10.1039/C4CC08057B
44. Qazi, S., Miettinen, H.M., Wilkinson, R.A., McCoy, K., Douglas, T., Wiedenheft, B.: Programmed self-assembly of an active P22-Cas9 nanocarrier system. Mol. Pharm. **13**, 1191–1196 (2016). https://doi.org/10.1021/acs.molpharmaceut.5b00822
45. Douglas, T., Young, M.: Host–guest encapsulation of materials by assembled virus protein cages. Int. J. Sci. **393**, 1996–1999 (1998)
46. Nassal, M., Schaller, H.: Hepatitis B virus replication. Trends Microbiol. **1**, 221–228 (1993). https://doi.org/10.1016/0966-842X(93)90136-F
47. Purohit, P.K., Inamdar, M.M., Grayson, P.D., Squires, T.M., Kondev, J., Phillips, R.: Forces during bacteriophage DNA packaging and ejection. Biophys. J. **88**, 851–866 (2005). https://doi.org/10.1529/BIOPHYSJ.104.047134

48. Llauró, A., Luque, D., Edwards, E., Trus, B.L., Avera, J., Reguera, D., Douglas, T., de Pablo, P.J., Castón, J.R.: Cargo–shell and cargo–cargo couplings govern the mechanics of artificially loaded virus-derived cages. Nano **8**, 9328–9336 (2016). https://doi.org/10.1039/c6nr01007e
49. Klug, W., Bruinsma, R., Michel, J.-P., Knobler, C., Ivanovska, I., Schmidt, C., Wuite, G.: Failure of viral shells. Phys. Rev. Lett. **97**, 228101 (2006). https://doi.org/10.1103/PhysRevLett.97.228101
50. Cieplak, M., Robbins, M.O.: Nanoindentation of 35 virus capsids in a molecular model: relating mechanical properties to structure. PLoS ONE **8**, e63640 (2013). https://doi.org/10.1371/journal.pone.0063640
51. Michel, J.P., Ivanovska, I.L., Gibbons, M.M., Klug, W.S., Knobler, C.M., Wuite, G.J.L., Schmidt, C.F.: Nanoindentation studies of full and empty viral capsids and the effects of capsid protein mutations. Proc. Natl. Acad. Sci. USA **103**(16), 6184–6189 (2006)